Journal Name

ARTICLE TYPE

Cite this: DOI: 00.0000/xxxxxxxxxx

Cucurbit[8]uril-mediated Pseudo[2,3]Rotaxanes†

Guanglu Wu,[a] István Szabó,[b] Edina Rosta,[b] and Oren A. Scherman[a]*

Received Date
Accepted Date

DOI: 00.0000/xxxxxxxxxx

Pseudo[2,3]rotaxanes have been successfully fabricated by the complexation of cucurbit[8]uril (CB[8]) macrocycles with extended viologen derivatives. Two design rules enable the incorporation of a third CB[8] onto a recently reported pseudo[2,2]rotaxane. Incorporation of a third macrocycle confines the dimeric stacking of chromophores into specific alignment, leading to effective electron-delocalisation along their long molecular axis.

Cucurbit[*n*]urils (CB[*n*]s, n = 5,6,7,8, and 10) are a class of synthetic macrocyclic molecules that can recognise a wide range of guest molecules with strong affinities, particularly in aqueous solution.[1,2] Depending on their cavity size, different CB[*n*] homologues bind with guests containing specific moieties. For instance, a phenyl or *p*-tolyl group has the perfect size and shape to fit a CB[7] cavity, resulting in a strong and "static" (on the NMR timescale) complexation.[3] CB[8], with a larger cavity volume, can simultaneously include two guest components, forming a ternary complex.[4,5] This ternary motif has been widely used as a bridging unit to link together two objects such as charge-transfer pairs,[4,6,7] peptides and proteins,[8,9] polymers,[10] particles,[11,12] and even macroscopic materials and surfaces.[13,14]

Recently, a 2:2 motif containing two rigid and elongated molecules, constrained by two CB[8] macrocycles,[15,16] has attracted increasing attention on account of its emerging features such as red-shifted absorption,[15,17] enhanced emission,[17–19] excimer formation,[17] directional self-sorting,[20] and a negative pKa shift.[21] This motif appears similar to pseudorotaxanes but contains more than one long-axis molecules; Cao *et al.* termed such structures as pseudo[*n*,*m*]rotaxanes,[19] where '*n*' is the number of long-axis molecules and '*m*' is the number of macrocycles in the complex. Therefore, a 2:2 complex can be described as a pseudo[2,2]rotaxane and a 2:3 complex containing three CB[8] macrocycles would be called a pseudo[2,3]rotaxane of CB[8].

CB[8]-mediated ternary complexes are generally dynamic structures in aqueous solution and typically display unresolved signals in the NMR spectrum. A pseudo[2,2]rotaxane, however, is extremely 'static' in aqueous solution with well-resolved NMR signals, although it seems like a simple connection of two ternary motifs.[15,17] As a result, formation of pseudo[2,2]rotaxanes offer a straightforward way to bring two molecules close to each other and remain in a stacked orientation for a long period of time, which facilitates the study of short-range, yet non-instantaneous interactions within a discrete dimer. We attribute the static feature of these dimers to the presence of a double CB[8] constrained system, which suppresses dissociation of the two long-axis molecules. Therefore, we posit that a pseudo[2,3]rotaxane with three CB[8] macrocycles may produce an even more static dimer by the introduction of an additional constraint.

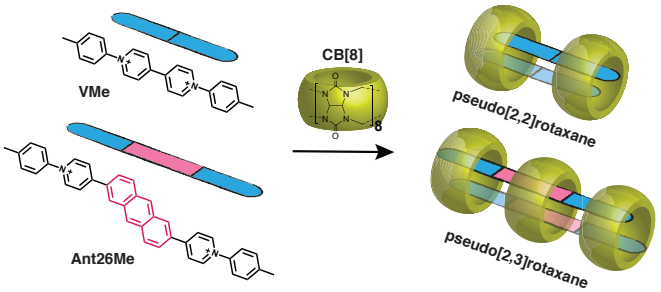

Fig. 1 Evolution from a pseudo[2,2]rotaxane to a pseudo[2,3]rotaxane of CB[8] by incorporating an elongated core into a diarylviologen. The Cl^- counterions are omitted for clarity.

The most straightforward route to a pseudo[2,3]rotaxane is to identify a pseudo[2,2]rotaxane with CB[8] and extend the length of its long-axis molecules by incorporating an elongated core. As shown in Fig. 1, a 2,6-anthracenyl moiety is inserted into the centre of a diarylviologen (**VMe**) motif, which has previously been reported to form a 2:2 complex with CB[8].[15] Preparation of the designed guest molecule, **Ant26Me**, starts with

[a] *Melville Laboratory for Polymer Synthesis, Department of Chemistry, University of Cambridge, Lensfield Road, Cambridge, CB2 1EW, UK.; E-mail: oas23@cam.ac.uk*
[b] *Department of Chemistry, King's College London, 7 Trinity Street, London, SE1 1DB, UK.*

† Electronic Supplementary Information (ESI) available: [details of any supplementary information available should be included here]. See DOI: 00.0000/00000000.

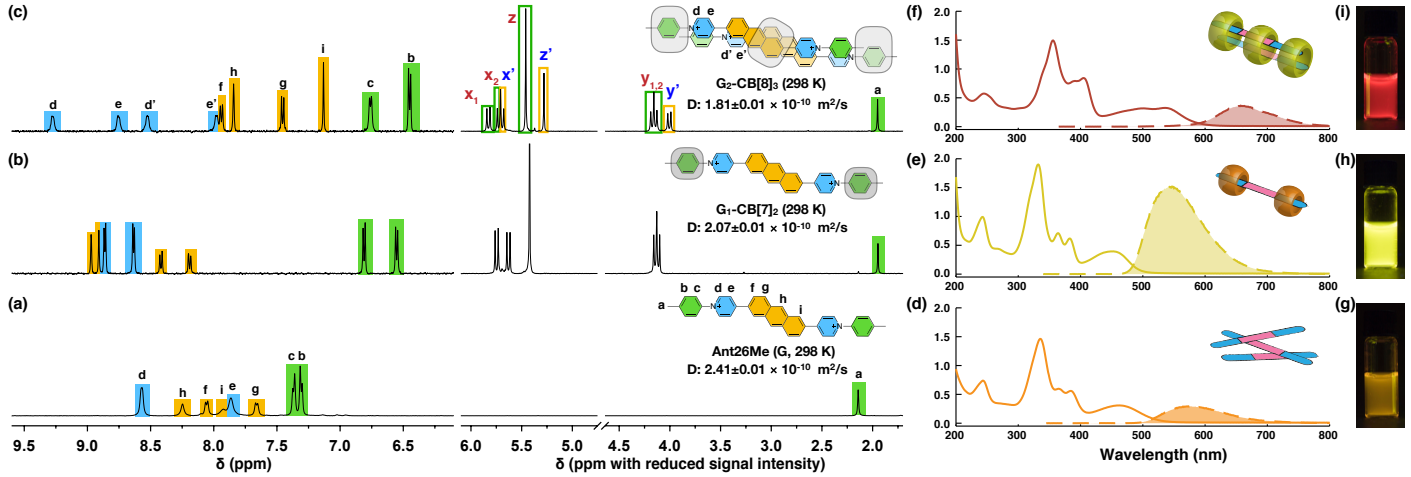

Fig. 2 ^{1}H-NMR (a,b,c), absorption/emission spetra (d,e,f), and photographs of solutions excited by a 365 nm lamp (g,h,i) for **Ant26Me** (G), G_1-CB[7]$_2$, and G_2-CB[8]$_3$, respectively, at 298 K. Emission spectra were obtained by excitation at the maximum absorption wavelength of each species between 330 nm and 360 nm. Concentrations of G are 500 μM in (a) and 65 μM in (b) and (c) for NMR studies, 10 μM for absorption measurements, and 30 μM for emission measurements as well as solutions depicted in the photographs. For a clear comparison, the intensity of the signals in the NMR spectra between 1.7 ppm and 6.0 ppm has been reduced.

Suzuki-Miyaura cross-coupling[22] of two pyridin-4-yl groups onto the 2,6-anthracenyl core followed by further transformation of the pryidin-4-yl moieties into tolylpyridinium salts through a Zincke reaction[17,23] (Scheme S2). We wondered if the two 1-(*p*-tolyl)pyridin-1-ium moieties would still behave as "clamping" modules to capture two CB[8]s in a dimeric manner while meanwhile exhibiting additional spacing to hold a third macrocycle.

A mixture of 2 equiv. **Ant26Me** with 3 equiv. CB[8] in D_2O results in a well-resolved ^{1}H-NMR spectrum (Fig. 2c) where each signal is assigned through variable-temperature NMR as well as COSY and NOESY 2D NMR (Fig. S2-S4). All the peaks exhibit a unified diffusion coefficient (D) of 1.81×10^{-10} m^2/s measured from DOSY experiments (Fig. S5), indicating that there is only one species in solution with a stoichiometric ratio of 2:3, *i.e.* G_2-CB[8]$_3$ (where G represents a guest molecule). Two sets of signals ($H_{x,y,z}$, $H_{x',y',z'}$) are observed in the range between 4.0 ppm and 6.0 ppm suggesting the presence of two types of CB[8] macrocycles in one complex. One set of CB[8] peaks exhibit a signal intensity (or integration) that is twice as large as the other (*e.g.* H_z *vs.* $H_{z'}$). This corresponds to two CB[8]s that are bound with tolyl groups from both ends as the CB[8] protons only exhibit cross-correlation NOESY signals with protons from tolyl moieties such as [H_z, $H_{a,b,c}$] (Fig. S4). Since the two portals of this type of CB[8] are exposed to an asymmetric chemical environment, their methylene protons display a characteristic split pattern,[15] *i.e.* $H_{x1,x2,y1,y2}$. On the other hand, a different CB[8] environment arises from the macrocycle that must be binding with the anthracenyl cores, as its protons ($H_{x',y',z'}$) only display cross-correlation NOESY signals with $H_{f,g,h,i}$ rather than $H_{a,b,c}$ (Fig. S4). Moreover, no signal splitting is observed for this CB[8], which is consistent with symmetric CB[8] portals in proximity to the central core. Compared to the spectrum of unbound **Ant26Me** (Fig. 2a), the upfield shift of tolyl and anthracenyl protons as well as the downfield shift of pyridinium protons also confirm the formation of a pseudo[2,3]rotaxane with two CB[8]s complexing the tolyl ends and an additional CB[8] held in between surrounding the anthracenyl cores.

One may notice that two pyridinium signals ($H_{d,e}$ in Fig. 2) are split into four peaks upon forming the pseudo[2,3]rotaxane with CB[8] ($H_{d,d',e,e'}$ in Fig. 2); this is not observed upon complexation with CB[7] as a G_1-CB[7]$_2$ complex(Fig. 2). A sharpening of these split signals is observed as the temperature is decreased (Fig. S2), which indicates slow interconversion on the NMR timescale between two degenerate states. This further suggests restricted intra-complex motion caused by triply-constrained dimeric stacks in the pseudo[2,3]rotaxane. The strong constraint applied by the presence of three macrocycles not only maintains the two long-axis molecules as a discrete and static dimer in aqueous solution but also confines their stacking in a controlled alignment, which leads to unique photophysical properties. As shown in Fig. 2d-i, the G_1-CB[7]$_2$ complex ensures a discrete monomeric state of **Ant26Me** displaying a bright yellow fluorescence. The aqueous solution of free **Ant26Me** molecules without any CB macrocycles exhibits a light orange emission, suggesting a certain degree of aggregation in water, which is further confirmed by its concentration-dependent NMR spectra (Fig. S6). The formation of a pseudo[2,3]rotaxane of **Ant26Me** with CB[8] shows a significant bathochromic-shift in both absorption and emission, displaying a bright red emission and a broad spectrum window of 300 nm between the excitation peak at 355 nm and emission peak at 657 nm. This large spectral shift suggests a substantial extent of electron-delocalisation on account of the dimeric stacking along the long molecular axis, which cannot happen without the confinement and protection from three CB[8] macrocycles. On the other hand, the free **Ant26Me** molecules can also stack into aggregates, but only in an arbitrary manner without a well-defined directional alignment of the anthracenyl cores (Fig. 2d).

Replacing the 2,6-anthracenyl core by a shorter 2,6-naphthyl moiety, **Np26Me** also results in the formation of a pseudo[2,3]rotaxane with CB[8] (Fig. S7). Moreover, it can form

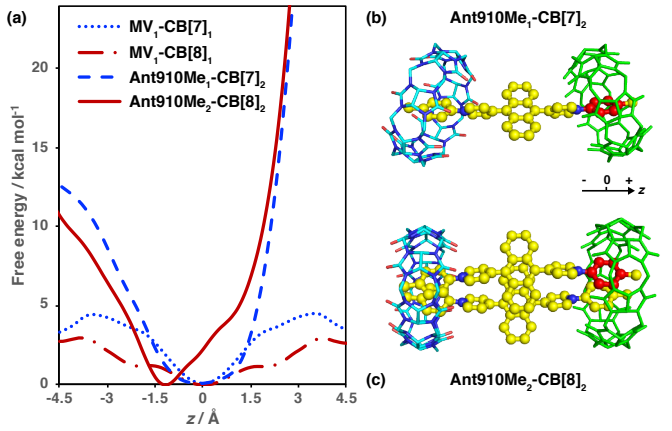

Fig. 3 Free energy profiles obtained from the Adaptive Biasing Force (ABF) method[24,25] correlated to the distance z between the centre-of-mass (COM) of CB[n] and the COM of the binding motif (a) for MV_1-CB[7]$_1$ (blue dotted line, MV represents methyl viologen), MV_1-CB[8]$_1$ (red dash-dotted line), Ant910Me$_1$-CB[7]$_2$ (blue dashed line), and **Ant910Me**$_2$-CB[8]$_2$ (red solid line). For **Ant910Me**$_1$-CB[7]$_2$ (b), z is the COM spacing between one phenyl moiety (highlighted in red) and CB[7] (green); while for **Ant910Me**$_2$-CB[8]$_2$ (c), z is the COM spacing between the phenyl moiety of one long-axis molecule (highlighted in red) and CB[8] (green).

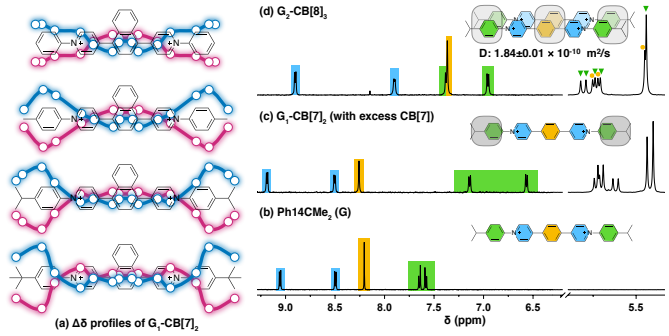

Fig. 4 Profiles established from the change in chemical shift of **Np14R** (R = H, Me, CMe_2, CMe_3) upon complexation with CB[7] (a) showing a central spacing determined by the size of the substituent R group. ^{1}H-NMR spectra for **Ph14CMe$_2$** (G), G$_1$-CB[7]$_2$ with excess CB[7], and G$_2$-CB[8]$_3$ at 298 K. Concentrations of G for all species are 60 μM. The blue and red profiles in (a) are plotted to highlight the chemical shift change for protons above and below the long-axis molecules, respectively. Specific values can be found in Fig. S9-S12.

a pseudo[2,1]rotaxane quantitatively in a mixture of 1 equiv. CB[8] and 2 equiv. **Np26Me**, displaying absorption and emission spectra similar to that of its pseudo[2,3]rotaxane (Fig. S8) on account of the same dimeric stacking. However, the mixture of 1 equiv. CB[8] and excess **Ant26Me** ($\geq$ 2 equiv) leads to a co-existence of several complexes in competition. Further shortening the central core to a 1,4-phenyl moiety, **Ph14Me** does not lead to the formation of a pseudo[2,3]rotaxane with CB[8] as it only forms a pseudo[2,2]rotaxane.[17]

Interestingly, while two **Ant26Me** or **Np26Me** molecules are capable of complexing three CB[8] macrocycles, a single long-axis molecule can only form a pseudo[1,2]rotaxane with two CB[7] macrocycles binding at the tolyl ends (Fig. 2b, Fig. S7) and is not able to complex three macrocycles even in the presence of a large excess of CB[7]. This indicates that the stacking of two long-axis molecules must result in a discrete entity that is considerably longer than its single molecule component. A molecular dynamics (MD) simulation demonstrates that the two long-axis molecules are actually stacked on top of one another with a slippage angle smaller than 90° resulting in only a partial overlap. As shown in Fig. 3, a 9,10-anthracenyl (**Ant910Me**) moiety is employed as the central core in order to prevent the CB[n] from shuttling across the central core (with a substantial energy barrier at $z > 1.5$ Å). In a **Ant910Me**$_1$-CB[7]$_2$ complex, the minimum free energy appears when moving the centre of the red highlighted phenyl moiety close to the centre of CB[7] ($z = 0$ Å). In a **Ant910Me**$_2$-CB[8]$_2$ complex, by fixing the related position between one long-axis molecule and CB[8], a minimum energy is obtained only when the red highlighted phenyl moiety of the movable long-axis molecule is placed slightly further away from the centre of CB[8] ($z < 0$ Å). This partial overlap in stacking of the two long-axis molecules leads to an elongated entity.

On the other hand, increasing the slippage between the two long-axis molecules may be possible through an alternative route, specifically by adjusting the steric demands at the end groups to arrive at a pseudo[2,3]rotaxane. Moreover, a larger end group may further extend the central spacing by pushing the two outer macrocycles away from the central core. This is demonstrated by a study of the complexation between CB[7] and a series of long-axis molecules (**Np14R**) containing 1,4-naphthyl cores and various end groups (R = H, Me, CMe_2, CMe_3) (Fig. S9-S12). In the NMR spectrum of a CB complexation, protons residing inside the centre of the CB cavity typically exhibit an upfield chemical shift of ca. 1 ppm, while protons located outside and proximate to the CB portals will display downfield shifts.[26] It is thus possible to determine the precise binding site by comparing proton chemical shifts before and after complexation with CB. **Np14R**$_1$-CB[7]$_2$ complexes are perfect for such analysis as CB[7] macrocycles in these systems are relatively static on the NMR timescale. The 1,4-naphthyl moiety does not allow for shuttling of CB[7] across the central core.[17] Furthermore, the tolyl end group possesses a perfect shape to trap CB[7] with an energy barrier larger than that in a typical methyl viologen-CB[7] complex, as shown in Fig. 3a. Therefore, we are able to generate a profile by plotting the change in chemical shift for each proton in **Np14R**, enabling a direct visualisation of the binding sites for CB[7] as shown in Fig. 4a. The dumbbell shape of each profile clearly shows the binding position of each CB[7] along the axis molecule, **Np14R**. It confirms that more bulky end groups generate larger central spacing.

Several new long-axis molecules containing a 1,4-phenyl core and bulkier end groups such as isopropyl (**Ph14CMe$_2$**) and tert-butyl (**Ph14CMe$_3$**) were synthesised in order to check if they form pseudo[2,3]rotaxanes even without an elongated core. The 1,4-naphthyl moiety was not used in this case as dimeric stacking of these cores is too large for simultaneous inclusion in a CB[8] cavity. Additionally, a tert-butyl group is too big to generate a dimeric entity with CB[8]. Instead, only pseudo[1,2]rotaxanes or pseudo[1,1]rotaxanes are observed in a mixture of 1 equiv.

Ph14CMe$_3$ with 2 equiv. or 1 equiv. CB[8], respectively (Fig. S13). However, a pseudo[2,3]rotaxane was successfully fabricated when using **Ph14CMe$_2$** as the long-axis molecule, exhibiting two types of CB[8] signals in Fig. 4d as well as a diffusion coefficient similar to those measured for **Ant26Me$_2$**-CB[8]$_3$. The D value of 1.84×10^{-10} m^2/s is smaller than the typical D value for complexes containing two CB[8] macrocycles,[27] suggesting a resultant complex with more than two CB[8]s. A thermogram (Fig. S15) obtained from isothermal titration calorimetry displays an obvious inflection point at a **Ph14CMe$_2$**/CB[8] ratio of around 0.67 corresponding to a stoichiometric ratio of 2:3. A 2:2 complex typically exhibits an enthalpy change of only around 80 kJ/mol;[15] while the large enthalpy change of around 110 kJ/mol before this inflection point suggests that two **Ph14CMe$_2$** long-axis molecules capture more than two CB[8] macrocycles. It is worth noting that a single Ph14CMe2 alone cannot complex three CB[7] macrocycles even in the presence of excess CB[7] (Fig. S14), which indicates that an increase of bulkiness at the termini not only extends the molecular surface along the long-axis of the dimer, but more importantly enlarges the slippage between the two long-axis molecules to ensure adequate central spacing for the third CB[8] macrocycle.

In conclusion, a discrete dimer consisting of two long-axis molecules with proper central spacing is critical for the formation of CB[8]-mediated pseudo[2,3]rotaxanes. This work demonstrates that extended central spacing can be realised not only through the incorporation of an elongated core unit such as a 2,6-anthracenyl or 2,6-naphthyl moiety, but also by utilising appropriate bulky end groups such as isopropyl moieties, which serve to push the outer two macrocycles away from the central core. The resultant pseudo[2,3]rotaxanes confine the stacked dimers of chromophores in a controlled manner leading to unique, emergent photophyscial properties.

This work was supported by the Leverhulme Trust (project: "Natural material innovation for sustainable living", G.W.), an EPSRC Programme Grant (NOtCH, EP/L027151/1, E.R., O.A.S.), and an ERC-2016 Consolidator Grant (CAM-RIG, 726470, O.A.S.), EPSRC (EP/R013012/1, EP/N020669/1), BBSRC (BB/N007700/1), and an ERC Starting Grant (BioNet,757850, I.S., E.R.). The authors thank Dr Magdalena Olesińska for offering 1,4-naphthyl precursors for Zincke reactions.

Conflicts of interest

There are no conflicts to declare.

References

1 S. J. Barrow, S. Kasera, M. J. Rowland, J. del Barrio and O. A. Scherman, Chem. Rev., 2015, **115**, 12320–12406.
2 K. I. Assaf and W. M. Nau, Chem. Soc. Rev., 2015, **44**, 394–418.
3 M. Freitag, L. Gundlach, P. Piotrowiak and E. Galoppini, J. Am. Chem. Soc., 2012, **134**, 3358–3366.
4 H.-J. Kim, J. Heo, W. S. Jeon, E. Lee, J. Kim, S. Sakamoto, K. Yamaguchi and K. Kim, Angew. Chem. Int. Ed., 2001, **40**, 1526–1529.
5 L. M. Heitmann, A. B. Taylor, P. J. Hart and A. R. Urbach, J. Am. Chem. Soc., 2006, **128**, 12574–12581.
6 Y. Liu, Y. Yu, J. Gao, Z. Wang and X. Zhang, Angew. Chem. Int. Ed., 2010, **49**, 6576–6579.
7 F. Biedermann and O. A. Scherman, J. Phys. Chem. B, 2012, **116**, 2842–2849.
8 A. R. Urbach and V. Ramalingam, Isr. J. Chem., 2011, **51**, 664–678.
9 C. Hou, X. Zeng, Y. Gao, S. Qiao, X. Zhang, J. Xu and J. Liu, Isr. J. Chem., 2018, **58**, 286–295.
10 E. A. Appel, F. Biedermann, U. Rauwald, S. T. Jones, J. M. Zayed and O. A. Scherman, J. Am. Chem. Soc., 2010, **132**, 14251–14260.
11 J. Zhang, R. J. Coulston, S. T. Jones, J. Geng, O. A. Scherman and C. Abell, Science, 2012, **335**, 690–694.
12 Y. Lan, Y. Wu, A. Karas and O. A. Scherman, Angew. Chem. Int. Ed., 2014, **53**, 2166–2169.
13 Y. Ahn, Y. Jang, N. Selvapalam, G. Yun and K. Kim, Angew. Chem. Int. Ed., 2013, **52**, 3140–3144.
14 J. Liu, C. S. Y. Tan and O. A. Scherman, Angew. Chem. Int. Ed., 2018, **57**, 8854–8858.
15 G. Wu, M. Olesińska, Y. Wu, D. Matak-Vinkovic and O. A. Scherman, J. Am. Chem. Soc., 2017, **139**, 3202–3208.
16 B. Yang, S.-B. Yu, H. Wang, D.-W. Zhang and Z.-T. Li, Chem. Asian J., 2018, **13**, 1312–1317.
17 M. Olesińska, G. Wu, S. Gómez-Coca, D. Antoón-Garciía, I. Szabó, E. Rosta and O. A. Scherman, Chem. Sci., 2019, **10**, 8806–8811.
18 S. Schoder, H. V. Schröder, L. Cera, R. Puttreddy, A. Güttler, U. Resch-Genger, K. Rissanen and C. A. Schalley, Chem. Eur. J., 2019, **25**, 3257–3261.
19 B. Zhang, Y. Dong, J. Li, Y. Yu, C. Li and L. Cao, Chin. J. Chem., 2019, **37**, 269–275.
20 K. Kotturi and E. Masson, Chem. Eur. J., 2018, **24**, 8670–8678.
21 H. Yin, Q. Cheng, R. Rosas, S. Viel, V. Monnier, L. Charles, D. Siri, D. Gigmes, O. Ouari, R. Wang et al., Chem. Eur. J., 2019.
22 T. K. Ronson, W. Meng and J. R. Nitschke, J. Am. Chem. Soc., 2017, **139**, 9698–9707.
23 D. Bongard, M. Möller, S. N. Rao, D. Corr and L. Walder, Helv. Chim. Acta, 2005, **88**, 3200–3209.
24 E. Darve, D. Rodríguez-Gómez and A. Pohorille, J. Chem. Phys., 2008, **128**, 144120–144133.
25 J. Henin, G. Fiorin, C. Chipot and M. L. Klein, J. Chem. Theory Comput., 2009, **6**, 35–47.
26 W. L. Mock and N. Y. Shih, J. Org. Chem., 1986, **51**, 4440–4446.
27 G. Wu, D. E. Clarke, C. Wu and O. A. Scherman, Org. Biomol. Chem., 2019, **17**, 3514–3520.